Jämsä-Jounela, Sirkka-Liisa; Gomez Fuentes, Jose; Hearle, Jonathan ; Moseley, David; Smirnov, Alexander

Control strategy for a multiple hearth furnace in kaolin production

Published in:
Control Engineering Practice

DOI:
10.1016/j.conengprac.2018.08.020

Published: 01/12/2018

Document Version
Publisher's PDF, also known as Version of record

Control Engineering Practice 81 (2018) 18–27

Contents lists available at ScienceDirect

Control Engineering Practice

journal homepage: www.elsevier.com/locate/conengprac

Control strategy for a multiple hearth furnace in kaolin production

Sirkka-Liisa Jämsä-Jounela [a], Jose Valentin Gomez Fuentes [a,*], Jonathan Hearle [b], David Moseley [b], Alexander Smirnov [a]

[a] Department of Chemical and Metallurgical Engineering, Aalto University, P.O. Box 16100, FI-00076 Espoo, Finland
[b] Imerys Minerals Par Moor Center, Par Moor Road, Par PL242 SQ, England, United Kingdom

ARTICLE INFO

Keywords:
Calcination
Advanced control
Soft sensor
Control performance
Multiple hearth furnace
Energy consumption
Quality

ABSTRACT

In the face of strong competition, the kaolin calcination industry is aiming at higher profitability through increased productivity and reduction of costs. Specifically, the industry is facing market demands to maintain product quality with the depletion of high-quality ore. Therefore, considerable research is being conducted to enhance existing processes and their operation and control. In this paper, the concept of a mineralogy-driven control strategy for multiple hearth furnaces for kaolin production is presented and discussed. The aim of the advanced control concept is to increase capacity and to reduce energy consumption while maintaining the desired product quality. The control is based on two main soft sensors: the spinel phase reaction rate indicator for energy use reduction and the mullite content indicator for capacity improvement. In this simulation study, the control strategy is tested and compared with an industrial controller based on a proportional–integral scheme as a benchmark. The results show that the capacity of the process is considerably improved and energy use is remarkably reduced.

1. Introduction

Kaolin is an important industrial clay mineral used in multiple products such as paper, rubber, paint, and refractory items. Various applications of kaolin require calcination to enhance clay mineral properties and to provide added value to the material. Calciner furnaces such as rotary kilns and multiple hearth furnaces (MHF) are widely used in industry for the calcination of kaolin. The calciner control system plays a major role in ensuring uniform product quality while maximizing furnace capacity and improving furnace energy efficiency for optimal operation.

Although the different applications place specific requirements on the properties of kaolin, the degree and ease with which kaolin properties can be customized during refining varies with mineralogy. More specifically, the effect of ore mineralogy on product quality is twofold. First, various ore properties (such as particle size distribution, structure ordering, and some impurities) strongly affect the reaction rates and heat, thereby shifting the temperature profile in the furnace and the final product properties. Because it is difficult to measure the product characteristics and solid temperature profile in the furnace, the existing control strategies mostly attempt to maintain constant gas temperature using traditional control implementations such as proportional–integral–derivative (PID) controllers. These strategies help to attenuate the variations in the solid phase temperature and calcination reaction rates through the furnace. However, the variations in the solid phase are not eliminated completely because of the fluctuating ore types and mineralogy. Therefore, these strategies do not allow uniform product calcination.

The second effect of ore mineralogy on product quality concerns impurities that can directly affect the final product characteristics without influencing the operating conditions in the calciner. In particular, impurities containing iron are known to have a strong effect on product color, whereas the iron content is too low to disturb the energy balance and temperature profiles in the furnace. Hence, the in-situ distribution of different types of kaolin and their processing conditions need to be matched to demand in an optimal manner (Jaemsae-Jounela, Laine, Ruokonen, et al., 1998; Laine, Lappalainen, & Jämsä-Jounela, 1995).

Because the quality of the calcined product heavily depends on the temperature profile along the furnace, the stable desired temperature is acute for producing optimal quality products. However, controlling the temperature in an industrial calciner is very challenging because of various factors. Specifically, cross-coupling effects among the variables as well as between zones (hearths) increase the difficulties in maintaining the temperature profile. Thus, in many cases, the desired gas temperature profile cannot be efficiently maintained by controlling temperature

* Corresponding author.
E-mail addresses: sirkka-liisa.jamsa-jounela@aalto.fi (S.-L. Jämsä-Jounela), jose.gomezfuentes@aalto.fi (J.V. Gomez Fuentes), jonathan.hearle@imerys.com (J. Hearle), david.moseley@imerys.com (D. Moseley), alexander.smirnov@aalto.fi (A. Smirnov).

https://doi.org/10.1016/j.conengprac.2018.08.020
Received 23 January 2018; Received in revised form 24 May 2018; Accepted 28 August 2018
Available online 12 September 2018

independently using conventional single-input single-output PI control. Therefore, different control methods such as multivariable control, model predictive control (Stadler, Poland, & Gallestey, 2011), and artificial intelligence with neural networks and fuzzy logic (Järvensivu, Saari, & Jämsä-Jounela, 2001) have been applied to overcome this problem in the calciner control.

Galvez and de Araujo (1996) designed a controller for a large industrial electrical tubular oven, which was divided into six heating zones with temperature measurements on each zone. The multivariable controller was built by combining the pre-compensator and PI controllers. The high level of interaction observed between the zones was compensated by the implementation of the decouplers. Sauermann, Stenzel, Keesmann, and Bonduelle (2001) also described using decoupling methods to maintain the desired and stable temperature profile in a four-zone furnace. Similar to the method previously described, each zone was equipped with an individual power supply, resulting in the individual control of temperature. A mechanistic model was developed by the researchers that considered all thermal coupling effects between the zones. It was found that the state (temperature) at one zone was not only affected by the power source of that zone but also by the temperature of other zones. Hence, the decoupling controllers were implemented to compensate the thermal coupling effects between the neighboring zones, including the non-neighboring zones. This resulted in improved temperature stability.

Ramírez, Haber, Pea, and Rodrguez (2004) designed and tested a multiple-input multiple-output fuzzy controller with multiple rule bases to control the postcombustion process in a multiple hearth furnace. The authors used a mamdani-type inference system for the fuzzy logic controller (Viljamaa & Koivo, 1995). The fuzzy controller considers five variables: the control errors of temperatures in Hearths 4 and 6, the change of these errors, and the specific fuel consumption. Several disturbances were introduced to the furnace for testing, and the controller regulated the temperature of the Hearths 4 and 6 in the desired range in all cases. Gouveia et al. also developed a controller for a multiple hearth furnace in a Nickel reduction process (Gouveia, Lewis, Restrepo, Rodrigues, & Gedraite, 2009). The authors used multivariable model-predictive techniques to design the controller, where the control actions are calculated to compensate for the strong interactions and time delays that characterize this type of furnaces. The results showed a reduction in the variability of the furnace conditions and an increase in energy efficiency and recovery of nickel.

In brief, the aforementioned studies focused on the gas phase temperature profile control, which requires several sensors and actuating elements (heaters) to be distributed through a furnace. Nevertheless, little attention is given in the literature to the solid phase temperature and its control strategy.

To cope with varying ore mineralogy, this study presents an overall furnace control strategy concept, which aims to maximize capacity and to minimize the use of energy while meeting the quality requirements of the products. The main module of the system is the database, which contains the feed-type characteristics (e.g., Fe_2O_3), the setpoint values to the temperature profile controllers, and the feed rate of the furnace. The mullite content in the product is indirectly estimated by the soft sensor to maximize process capacity, a value higher than the threshold provides an opportunity to increase the feed rate. The stabilizing controllers manipulate the gas temperature to attenuate or compensate for variations in the calcination reactions in the solids. The feedforward controller adjusts the temperature setpoint in the last part of the furnace based on the soft-sensor values of the exothermic reaction rates in the first part of the furnace. Thus, the design of the proposed control strategy considers the effect of ore properties on the quality of the final product and the stabilizing control emphasizes the transition phase as the ore type and its mineralogy are changing.

The remainder of this manuscript is organized as follows. Section 2 describes the process and Section 3 provides the mechanistic model of the MHF. Section 4 describes the dynamic behavior of the process and analyzes the effect of ore mineralogy on the properties of the final product. The overall control strategy is also described. Section 5 presents the simulation results using the industrial data and ends with a discussion and analysis of the research. Finally, Section 6 concludes the manuscript.

2. Process description and control strategy

Calcination is the process of heating a substance in order to remove water from the structure of that substance. This process is one of the most important means of enhancing the properties and value of kaolin. As a result of calcination, the kaolin improves its physical properties such as its brightness, allowing it to be used in a wide variety of products, such as paper, rubber, paint and refractory items.

The MHF considered in this study has countercurrent solid and gas flows and consists of eight hearths. The thermal energy required for calcination is provided to the furnace through four methane burners located on hearths 4 and 6. The temperature in these locations is controlled by manipulating the fuel gas flow, which determines the quantity of combustion air. The furnace walls are built with bricks and circumscribed by a cylindrical steel shell with a refractory lining. Fig. 1 illustrates the cross-sectional view of the furnace. The material flow through the furnace is stirred spirally and transported across the hearths by a centrally located vertical rotating shaft carrying arms with rabble blades. Four arms are used on each hearth and each arm holds three to five rabble blades. The material is dispensed into the top hearth through a single inlet from the weigh feed hopper to the periphery of the hearth. Inside the odd-numbered hearths, the material is conducted by the rabble blades towards the center of the hearth and then descends to the hearth beneath from the center through a single annulus around the shaft. By contrast, the material in the even-numbered hearths is transported outwards before descending through the drop holes at the border of the hearth to the subsequent hearth. The transportation is repeated until the base hearth is reached, from which the calcined product is evacuated through the two exit holes.

Kaolin consists primarily of the mineral kaolinite, which has the formula $Al_2Si_2O_5(OH)_4$. During calcination, kaolin undergoes four physical–chemical processes as presented in Ptáček, Šoukal, Opravil, Havlica, and Brandštetr (2011). First, the evaporation of free moisture occurs ($T \leq 100$ °C).

$$H_2O(l) \rightarrow H_2O(g) \tag{1}$$

Next, kaolin undergoes a dehydroxylation reaction, in which the chemically bound water is removed and amorphous metakaolin is formed at 450 °C to 700 °C.

$$\underset{\text{Kaolinite}}{Al_2O_3 \cdot 2SiO_2 \cdot 2H_2O} \rightarrow \underset{\text{Metakaolin}}{Al_2O_3 \cdot 2SiO_2} + 2H_2O(g) \tag{2}$$

The third physical–chemical process involves a reaction leading to the transformation of metakaolin to the "spinel phase" by exothermic recrystallization at 925 °C to 1050 °C.

$$2(Al_2O_3 \cdot 2SiO_2) \rightarrow \underset{\text{Silicon-spinel}}{2Al_2O_3 \cdot 3SiO_2} + SiO_2(\text{amorphous}) \tag{3}$$

In the fourth and final process, the nucleation of the spinel phase occurs and the material transforms into mullite at a temperature above 1050 °C

$$2Al_2O_3 \cdot 3SiO_2 \rightarrow \underset{\text{1:1 mullite-type phase}}{(2Al_2O_3 \cdot SiO_2)} + SiO_2. \tag{4}$$

Mullite formation intensifies when the temperature increases to above 1400 °C

$$3(Al_2O_3 \cdot 2SiO_2) \rightarrow \underset{\text{3:2 mullite}}{3Al_2O_3 \cdot 2SiO_2} + SiO_2 \tag{5}$$

Mullite is hard and abrasive and, as a result, can cause damage to process equipment. The desired final consistent product, which is within the specification limits, has both a low mullite and metakaolin content. The

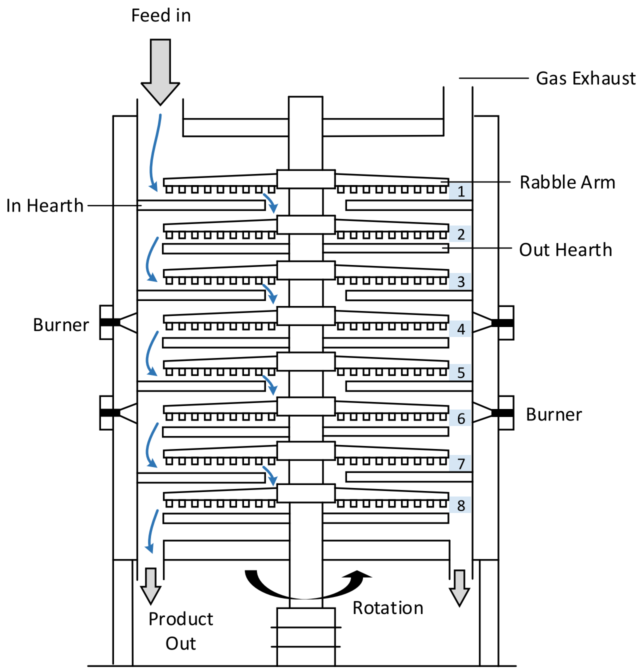

Fig. 1. Schematic of a cross section of an MHF. The numbers on the right denote the hearth numbers starting from material feed. The blue lines on the left show how the material flows from outside to the center on the odd-numbered hearths and in the reverse direction on the even-numbered hearths (Eskelinen, Zakharov, Jämsä-Jounela, and Hearle, 2015).

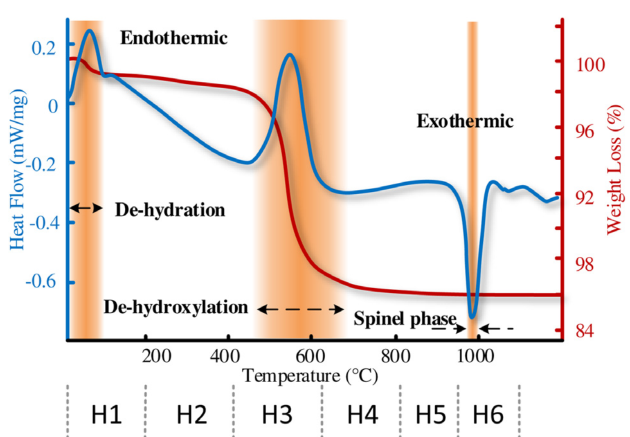

Fig. 2. Thermogravimetric analysis and differential scanning calorimetry curve for kaolin calcination (provided by IMERYS) (Eskelinen et al., 2015). The corresponding locations in the furnace are denoted.

differential scanning calorimetry (DSC) and thermogravimetric analysis (TGA) curves presenting the kaolin calcination are given in Fig. 2.

The reaction (1) proceeds in hearths 1 and 2. Starting from hearth 3, the temperature is sufficiently high to initiate the reaction (2) in which metakaolin is formed and a loss of weight (Dehydroxylation) occurs. This is displayed in the TGA curve shown in Fig. 2. DSC tests indicate that the reaction is endothermic, as denoted by the blue line in the same figure. The spinel form appears in hearths 5 and 6, after which the material is cooled in the last two hearths. The spinel formation reaction is exothermic, depicted in the temperature range of 925 °C to 1050 °C, and the crystal structure of the metakaolin transmutes to a more stable state (Ptáček et al., 2011). If the temperature profile is outside the specifications, the reaction (3) might start earlier and mullite will generate through the reaction (4).

The temperatures in hearths 4 and 6 are controlled by a PI scheme that adjusts the gas flows to the burners. These controllers maintain the temperatures within the safety limits. The measurements of gas and air flow are performed using orifice plate flow meters. The feed rate determines the maximum gas flow allowed in hearth 4, this constraint prevents an unnecessary use of gas. To ensure complete combustion of the gas, a sufficient amount of air is required, which is controlled by separate PI controllers. The setpoint for the combustion air flow is determined based on the stoichiometric ratio between the oxygen and methane in the combustion reaction. Decouplers were considered to be included as part of the temperature control, but due to the unavailability of actuators in hearth 5 the idea was dismissed.

3. Dynamic model of the multiple hearth furnace

Mechanistic models have proven to be an excellent tool for gaining deeper understanding of processes and their behavior. The development of the mechanistic model for the MHF is supported by numerous studies of the reactions related to kaolin calcination. For example, the fundamentals of kaolin calcination and classification of different calcined kaolin were introduced in Murray (2000) and Murray and Kogel (2005). Furthermore, the kinetics of kaolin calcination was examined by Ptáček et al. (2010, 2011), and both Castelein, Soulestin, Bonnet, and Blanchart (2001) and Langer and Kerr (1967) analyzed the effect of the heating rate on the properties of calcined kaolin. In addition, industrial experiments with tracer materials were used to examine the residence time distribution in the furnaces used for calcination such as the MHF (Thomas et al., 2009) and rotary kilns (Ferron & Singh, 1991; Gao et al., 2013).

Despite the abundance of research that has examined calcination reactions, considerable research is still required to quantitatively describe the phenomena occurring in the MHF calciner. In the literature, several mathematical models have been reported. Meisingset and Balchen (1995) developed a steady-state mechanistic model for a single hearth rotary coke calciner. Martins, Oliveira, and Franca (2001) described a one-dimensional steady-state model of petroleum coke calcination in a rotary kiln that predicts the temperature profiles for the bed, gas phase, and kiln wall in the axial direction. Voglauer and Jörgl (2004) presented a dynamic model of a multiple hearth furnace used for the roast process to recover vanadium. Liu and Jiang (2004) also developed a mathematical model related to mass and heat transfer in a continuous plate dryer. More recently, Ginsberg and Modigell (2011) developed a dynamic model of a rotary kiln used for calcinating titanium dioxide.

In this study, the dynamic model that is used to describe kaolin calcination in the MHF was presented in Eskelinen et al. (2015). The MHF is divided into six parts: gas phase, walls, the solid bed, central shaft, rabble arms, and the cooling air. The model of the furnace contains the mass and energy conservation equations for each of the six parts and comprises the kinetics of the reactions occurring in the solid phase. In addition, the model incorporates the equations used to calculate the parameters that affect the heat exchange between the different parts of the model, such as the solid and gas-bed emissivities, and the temperature dependent parameters such as the heat capacities of the gas components. The gas phase includes methane, oxygen, nitrogen, water, and carbon dioxide, whereas the solid bed includes water, kaolin, metakaolin, the spinel phase (product), and mullite (offspec).

The solid bed on each hearth is split into several annular volumes according to the configurations of the furnace rabble arms. To simplify the mass transfer dynamics inside the furnace, the volumes are considered homogeneous in composition and temperature, and all volumes in a hearth are assumed to be equal in width in the mass content and radial direction. The mixing model considers the distribution of the contents of a volume between itself and its neighboring volumes (i.e., the preceding and subsequent volumes) after one full shaft rotation.

The gas phase is considered to follow the ideal gas laws, and the difference between the pressure inside the furnace and the atmospheric

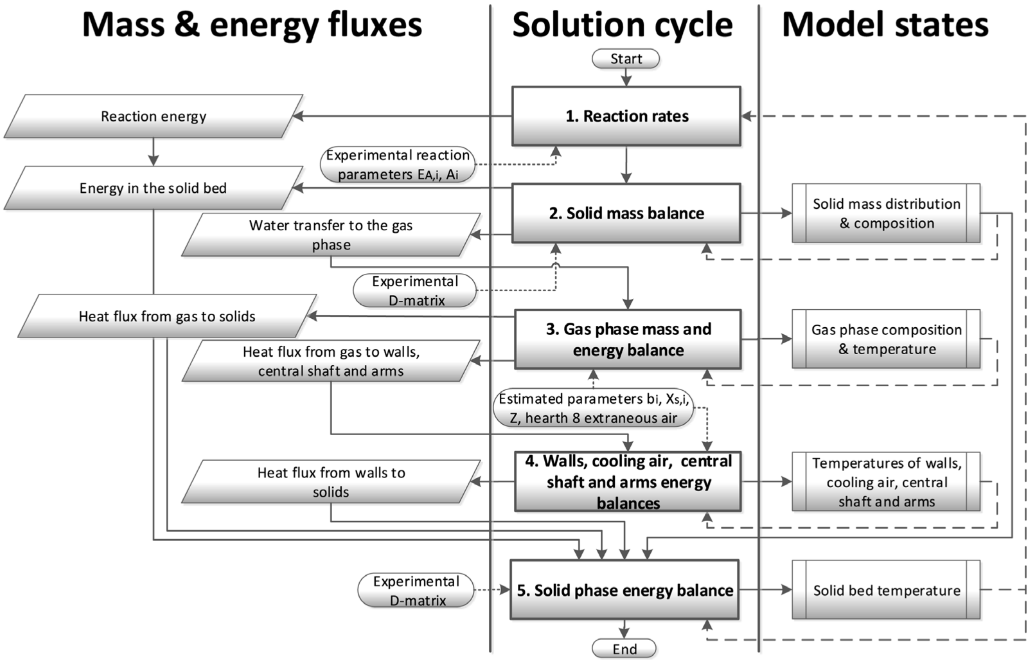

Fig. 3. Scheme of the solution for the MHF model (Eskelinen et al., 2015).

pressure is neglected. Similar to the solid bed, the gas phase is divided into annular volumes accordingly, assuming the gas volumes are homogeneous with respect to the temperature and composition. Because of the short residence time of the furnace, the gas phase can be described with steady-state modeling equations, and its temperature is defined by the temperature profiles of the other model components.

The following heat exchange paths are considered in the model: between gas and wall, wall and environment, gas and central shaft with the arms, solid and gas, and solid and wall. In addition, heat exchange occurs between the cooling air and central shaft with the rabble arms. Furthermore, heat conduction inside the walls in the radial horizontal direction is considered. The model uses the energy balances for the walls, central shaft, gas phase, rabble arms, cooling air, and solid bed to describe the temperature profile dynamics of the parts. Specifically, after the energy balance equations are initially resolved, the temperature values can be obtained.

The solution for the MHF model consists of the following steps. Initially, the reaction rates are determined using the reaction kinetics retrieved from experimental data and previous studies. Next, the solid mass distribution is computed according to the mixing model. Then, the mass and energy balances of the gas phase are solved using the temperature-dependent model parameters. In the next step, the energy balance calculations for the central shaft, walls, cooling air, and the rabble arms are performed. Finally, the mixing model is applied to solve the energy balance of the solid phase, which requires the heat fluxes estimated in the previous steps. A summary of the model solution cycle is presented in Fig. 3, which illustrates how the model states and computable parameters are used (Eskelinen et al., 2015). The solving algorithms are implemented in a MATLAB environment.

4. Analysis of the process dynamic behavior and control strategy development

4.1. Mullite content indicator for capacity improvement

During normal operation, the conditions inside the furnace allow 100% conversion of metakaolin to the spinel phase, at 925 °C (Eq. (3)). The metakaolin is transformed directly into mullite at a higher temperature of 1050 °C (Eq. (4)). Therefore, an inverse mass proportion exists between mullite and the spinel phase as the reaction progresses. Consequently, mullite can be considered as an indirect indicator of the quantity of the product. In other words, if the final product contains a considerable amount of mullite, the temperature inside the furnace is higher than the optimal, as the thermal conditions are more favorable for this reaction (Eq. (4)). The main objective of the control strategy is to maximize the capacity while maintaining the desired product quality. Then, monitoring the process conditions during mullite formation would provide a good opportunity and means to improve calcination by increasing the feed rate and decreasing the temperature (minimizing mullite formation), thus leading to optimal product quality.

Mullite content is not measured online. Therefore, in this study, a soft-sensor based on energy balances was defined to estimate the amount of mullite in the product. The energy balances were calculated based on the heat transfer flow across the furnace. The equations defining the energy balances are as follows:

$$\frac{\partial Q_{tot}}{\partial t} = Q_{comb} - Q_{loss} - Q_{gas} - Q_{air} - (Q_{solid} + Q_{mul}) = 0 \tag{6}$$

$$Q_{solid} = Q_{water} + Q_{kao} + Q_{dehyd} + Q_{meta} + Q_{spin} + Q_{prod} \tag{7}$$

where $\frac{\partial Q_{tot}}{\partial t}$ is the heat transfer rate, Q_{comb} is the total energy generated by combustion of methane from the burners, and Q_{loss} is the energy loss to the ambient through the furnace walls. In addition, the enthalpy of the net energy gained by the gas phase is denoted as Q_{gas}, the energy difference in the cooling air that flows through the central shaft is given as Q_{air}, the solid phase energy change is represented as Q_{solid}, and the total energy of mullite formation is defined as Q_{mul}. Furthermore, Q_{solid} is defined as presented in (7), where Q_{water} is the energy to evaporate free water, Q_{kao} is the energy to heat kaolin to 450 °C, Q_{dehyd} is the energy consumed as a result of the dehydroxylation reaction, Q_{meta} is the energy for heating metakaolin to 1000 °C, and Q_{spin} is the energy released during the spinel phase formation reaction. Finally, Q_{prod} is the heat released in order to cool the final product to 700 °C.

From Eq. (6), assuming the steady-state conditions, and all the variables of the equation being measurable, thus the total energy of mullite formation(Q_{mul}) is calculated as follows:

$$Q_{mul} = Q_{comb} - Q_{loss} - Q_{gas} - Q_{air} - Q_{solid} \tag{8}$$

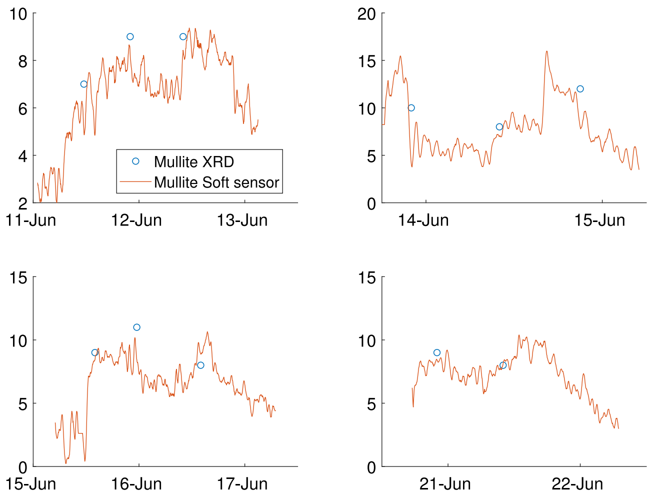

Fig. 4. Mullite content, XRD vs. the soft sensor estimation.

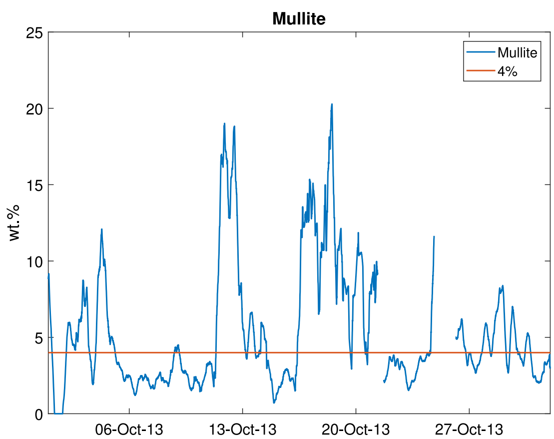

Fig. 5. Mullite content estimation from the energy balance for October 2013.

Then, the mass of mullite formed can be obtained as follows:

$$m_{mul} = \frac{Q_{mul}}{H_{mul}} \tag{9}$$

where m_{mul} is the mass of mullite formed, and H_{mul} is the formation enthalpy of mullite, which is obtained from the literature.

The equations for mullite content estimation were compiled as a soft sensor. Process data were used to obtain an estimation of the mullite content and compared with the chemical analyses of mullite content for the same period. The data was obtained from the samples gathered directly from the calciner during one month. This data includes the process variables from the history logs as well as the results from the chemical analyses such as X-ray Diffraction (XRD) for the mullite content. The results are presented in Fig. 4.

The estimated mullite content shows good accuracy with respect to the XRD results. The number of the samples is however limited and the results are thus preliminary, further research is needed with a longer sampling campaign.

The soft sensor was next applied to a set of industrial data of the furnace for the period of May to October of 2013. Data analysis for the period showed that during normal operating conditions, the content of mullite was maintained at 4% or less. This threshold was then compared to the results of the soft sensor for the month of October 2013 the graph for which is presented in Fig. 5. The high mullite content (over 4%) indicates non-optimal conditions for the process, implying temperatures of 1050 °C or higher and yielding a product with lower quality. Additionally, the feed rate was reported to be maintained below the maximum.

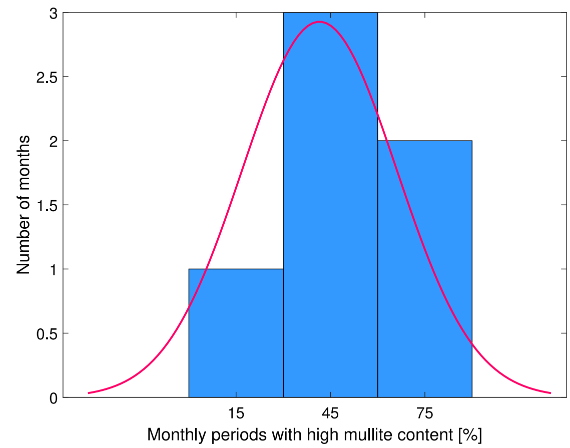

Fig. 6. Normal distribution of monthly time periods when mullite content is above 4% and the feed rate is below the maximum.

Fig. 6 shows a normal distribution of monthly time percentage when the mullite content was above the threshold value during the testing period, displaying an average of 45% per month. Based on the results, great improvement can be achieved by following the dynamic behavior of the mullite soft sensor and incorporating the information into a high-level control strategy.

4.2. Spinel phase reaction rate indicator for energy use reduction

Calcination of kaolin in an MHF is a temperature-dependent process, and control of the temperature profile ensures the quality of the product. Calcined kaolin in the spinel phase is the main product of the furnace and is formed by a highly exothermic reaction (3), which occurs in hearth 6. The change in the location of the reaction affects the quality of the product and, therefore, the temperature profiles should be monitored and controlled. However, the necessary measurements to investigate when the reactions of kaolin in the spinel phase occur are not available. As an alternative practical approach to solving this problem, a soft sensor was considered and developed to estimate the rate of the exothermic reaction occurring in hearth 4.

A data analysis demonstrated several instances where the gas flow in hearth 4 fluctuates together with the temperature measurements in hearth 5. Various ore properties (e.g., ore impurities, particle size), as well as the solid temperature strongly affect the initiation of Eq. (3). If the solid temperature is sufficiently high in hearth 4, then the "spinel-phase" exothermic reaction (Eq. (3)) may take place at this location. For example, a feedforward control with the spinel phase reaction indicator would offer a great opportunity to increase energy savings in the furnace. To demonstrate the energy savings opportunities, a data analysis for the period of May to October 2013 was performed and cases from the industrial data were recorded. As a result, the increased reaction rates were recognized. The instances of this occurrence are presented in Fig. 7. The fluctuation in the temperature in hearth 5 can be explained by the activation and deactivation of the exothermic reaction in hearths 4 and 5. The amount of gas required to maintain the temperature in hearth 4 decreases once the exothermic reaction initiates. When the exothermic reaction nears completion, a greater amount of gas is necessary to maintain the desired temperature. In summary, the increased reaction rate is recognized when the gas flow to hearth 4 drops as the gas temperature in hearth 5 increases.

For control of energy savings, a soft sensor that estimates the rate of the exothermic reaction occurring in hearth 4 is needed. Energy balances for the first four hearths are calculated according to the law of

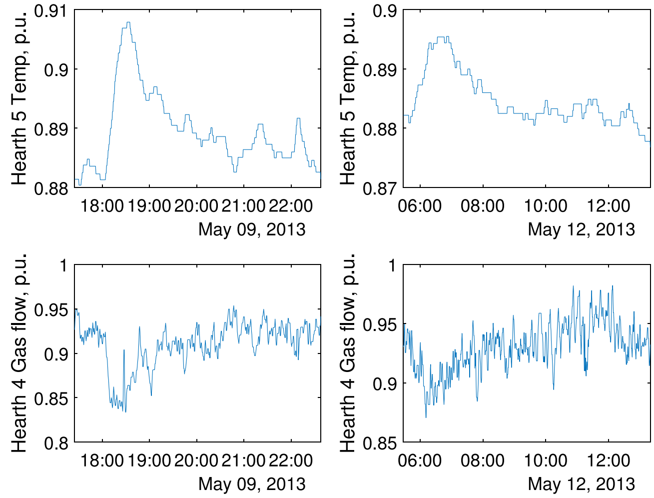

Fig. 7. Examples of activation and deactivation of the exothermic reaction in hearths 4 and 5.

energy conservation (Jenkins & Mullinger, 2013). Combustion energy of methane from hearth 4 and cooling air flow from hearth 5 are considered as inputs. The air required for complete combustion is estimated with the stoichiometric ratio of the fuel gas and air. The energy leaves the furnace through solids, exhaust gases, and heat losses, which include the cooling air and heat exchange with the surroundings.

The equations describing the energy balance for the solid and gas phases are given as follows.

$$\frac{\partial Q}{\partial t} = Q_{\mathrm{s,in}} - Q_{\mathrm{s,out}} - Q_{\mathrm{evap}} + Q_{\mathrm{dehyd}} + Q_{\mathrm{spin}} + Q_{\mathrm{sg}}, \tag{10}$$

$$Q_{\mathrm{g,in}} - Q_{\mathrm{g,out}} + Q_{\mathrm{comb}} - Q_{\mathrm{gs}} = 0, \tag{11}$$

where $\frac{\partial Q}{\partial t}$ is the rate of energy change with respect to time, enthalpies of the incoming and outgoing kaolin are denoted as $Q_{\mathrm{s,in}}$ and $Q_{\mathrm{s,out}}$, respectively; Q_{evap} is the energy of evaporated water; Q_{dehyd} is the energy consumed as a result of the dehydroxylation reaction, Q_{spin} is the energy released during the spinel phase formation reaction in hearth 4, and Q_{sg} is the energy transfer between the solid and gas phases. Enthalpies of the inflowing and outflowing gases are denoted as $Q_{\mathrm{g,in}}$ and $Q_{\mathrm{g,out}}$ respectively; Q_{comb} is the energy produced by combustion of methane from the burners in hearth 4, and Q_{gs} is the energy transferred between the solid and gas phases. Under the assumption of steady-state conditions, the rate of change is zero and the energy released by the spinel formation reaction is expressed as follows:

$$\begin{aligned} Q_{\mathrm{spin}} = & -Q_{\mathrm{s,in}} + Q_{\mathrm{s,out}} + Q_{\mathrm{evap}} + Q_{\mathrm{dehyd}} \\ & - \left(Q_{\mathrm{g,in}} - Q_{\mathrm{g,out}} + Q_{\mathrm{comb}}\right) \end{aligned} \tag{12}$$

Therefore, the exothermic rate of reaction ($R(t)$) is estimated as the percentage of kaolin transformed to the spinel phase in hearth 4

$$\mathrm{R}(t) = \frac{Q_{\mathrm{spin}}(t)}{H_{\mathrm{S}} F(t)}, \tag{13}$$

where H_{S} is the product formation heat and $F(t)$ is the current feed rate.

To finalize the data analysis, the exothermic reaction rates were estimated from the data available from May to October 2013. The soft sensor was used to identify the start, end, and duration of the spinel formation reaction (3) in the data. The mean duration of the reactions for the data studied was approximately 118 min with a minimum of 22 min and a maximum of 232 min. The phenomena have an effect on the total gas burned, generally decreasing the consumption in all cases by approximately 1.5% per hour.

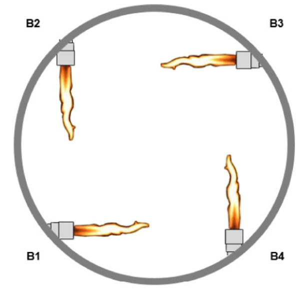

Fig. 8. Burner configuration in a MHF.

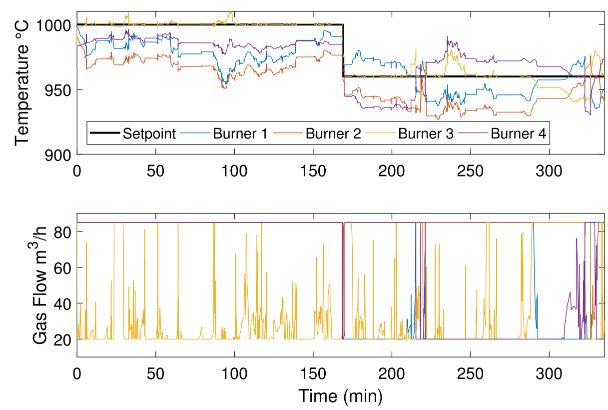

Fig. 9. Simulation results of the temperature setpoint change for the hearth 4 current temperature control.

4.3. Burner-to-burner interaction on the basic temperature control

There is pressure on industry to minimize NOx emissions in multi-burner furnaces. Therefore, improved burner technologies have been implemented to address this issue. Generally, these technologies adopt a type of furnace gas recirculation that minimizes the flame temperature, thereby decreasing the amount of NOx emissions. However, to lower the flame temperature, a reduction in the concentration of air is enforced which produces longer flames. Flames in modern multi-burner furnaces that have increased in length and volumetric heat release density might lead to a phenomenon known as burner-to-burner (BtoB) interaction (Fleifil, Lorra, Baukal, Lewallen, & Wright, 2006).

For the MHF, the configuration of the burners inside the furnace gives a clear view of the interactions inside the furnace. The configuration is disposed in four equidistant points around the circumference of the hearth. Every burner is located in one of the points and faces a contiguous burner, thus Burner 1 (B1) faces Burner 4 (B4), B4 faces Burner 3 (B3), etc., as presented in Fig. 8.

The control employed in hearths 4 and 6 consists of 4 PI controllers, one for each burner, operating individually. The possibility exists that an increased capacity operation may give rise to difficulties in controlling temperature in the MHF. These difficulties are most likely related to the BtoB phenomenon, which causes some instabilities and nonlinearities in the temperature control.

The current control strategy at the plant presents limitations when a BtoB phenomenon occurs during the process, causing undesired interaction and preventing smooth control of the gas phase temperature. In this study, this phenomenon was simulated and is depicted in Fig. 9. During the first 170 min of the simulation, the controller tries to follow the setpoint of 1000 °C with corresponding manipulated gas flows. After 170 min, the controller aims to follow a setpoint of 960 °C also with corresponding manipulated variables. For the first part (1000 °C setpoint), the temperature is reached only by one burner at a time,

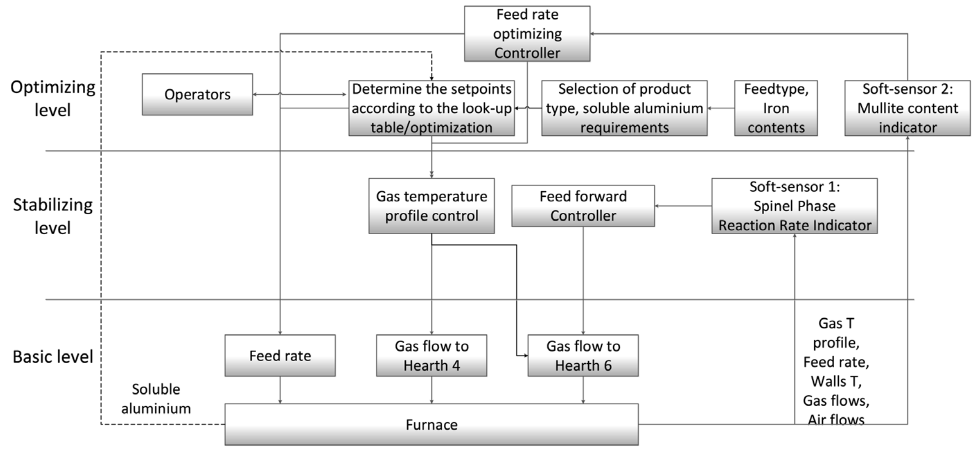

Fig. 10. Control scheme of the furnace.

with one control loop working. The second part shows that only one temperature follows the setpoint partially, with a switching of working control loops at simulation times of 220 min and 290 min. In this case study, one of the control loops works properly under a PI controller while the other controllers work in open loops where the gas flows are set to maximum.

4.4. Enhanced control strategy for the multiple hearth furnace

The overall control strategy proposed in this study, aims to select the best operating conditions to improve the production capacity and energy efficiency, and to achieve the required product quality. The process control system comprises the optimizing, stabilizing, and basic levels, as shown in Fig. 10.

The plant personnel determine the final product specifications while considering the current ore mineralogy. The product quality requirements (e.g., the soluble aluminum content and brightness) are defined next to the selected product specifications. A look-up table provides the setpoints for the gas temperatures in hearths 4 and 6 based on the current production capacity and iron content in the ore. The table is based on the classification of the feed type and process conditions utilizing the Self Organizing Map (SOM) technique (Jaemsae-Jounela et al., 1998; Laine et al., 1995). Furthermore, the temperature setpoints are adjusted on a regular basis (e.g., once a day) based on the laboratory measurements of the product characteristics, aiming to maintain the product quality within the specifications.

To achieve the maximum production rate, indicated by the mullite content soft sensor, the optimization problem is resolved to increase plant capacity (F) and simultaneously minimize the energy consumption ($F_4 + F_6$) by adjusting the temperature setpoint (T_6) in order to maintain the required mullite content (m).

$$max\ F \tag{14}$$

$$min\ (F_4 + F_6) \tag{15}$$

With respect to constraints:

$$F_{T4}(F_4, F_6, r, F) = T_4,$$
$$F_{T6}(F_4, F_6, r, F) = T_6,$$
$$m(F_4, F_6, T_1, F) \leq m^*,$$
$$S(F_4, F_6, r, F) \leq S^*,$$
$$T_6 \geq T_6^{min}(F, r),$$
$$T_4^{min} \leq T_4 \leq T_4^{max},$$

where F, F_4, and F_6 represent the kaolin feed rate and gas flows to hearths 4 and 6, respectively; r is the current value of the reaction soft sensor; T_1, T_4 and T_6 are the temperatures in hearths 1, 4 and 6, respectively; m and m^* are the mullite content and its threshold. Finally, S and S^* are the soluble aluminum content and its threshold (if applicable).

The stabilizing level aims to attenuate the variations in the calcination reaction that occur in the solid phase of the furnace. In other words, the gas temperature setpoints have to be modified based on the calcination progress in the solid phase. Thus, if the exothermic reaction starts when the material enters hearth 6 or occurs actively in hearth 4, the temperature setpoints must be lowered to save fuel and to avoid over-calcination. In order to assess the calcination progress, the soft sensor is used to estimate the exothermic reaction rate in hearth 4 and the feedforward control is used to adjust the temperature in hearth 6.

Controllers at the basic level shown in Fig. 10, control the temperature with a mean temperature control scheme. The mean temperature control aims to attenuate the effects of the BtoB phenomenon and homogenize the gas phase temperature in hearth 4 by operating on the average temperature of the gas phase instead of manipulating each burner individually.

5. Simulation results

5.1. Testing environment

The testing setup for modeling and control of the MHF was conducted in the MATLAB® environment. The setup consisted of the dynamic model of the MHF and controllers: basic temperature control, stabilizing control, and optimizing controllers. These included soft sensors: a mullite content indicator for capacity improvement and a spinel phase reaction rate indicator for energy use reduction. To speed up the computations, the mechanistic model was converted to the C language and precompiled. All other blocks and elements were realized using the standard MATLAB® functions. The simulation included an Euler solver with a fixed step of 20 s. A general overview of the simulation environment is presented in Fig. 11. The gas flows and temperatures present noise in the results which is estimated from the process data provided from May to October 2013. The testing focus of this study is the soft sensors which are the novel elements in the control strategy concept. The limited availability of online quality measurements restricts the testing of the control concept in closed loop and requires further online testing at the plant.

5.2. Simulation of basic temperature control

For BtoB interaction, a mean temperature control scheme was devised and tested for the hearth 4 case (Gomez Fuentes, 2016). By manipulating the total gas flow, a simulation of the mean control is

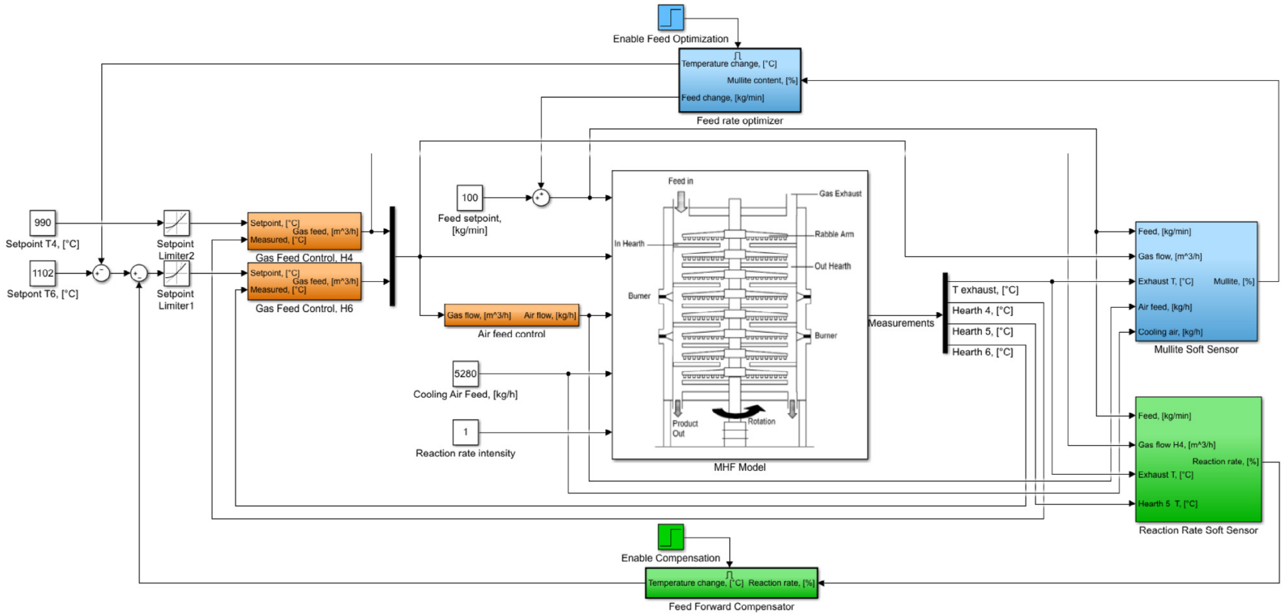

Fig. 11. Simulation environment of the control strategy. Blocks responsible for the basic control level (Fig. 10) are denoted in orange. The green blocks are related to the stabilizing level shown in Fig. 10. The optimizing level (Fig. 10) is presented in blue. (For interpretation of the references to color in this figure legend, the reader is referred to the web version of this article.)

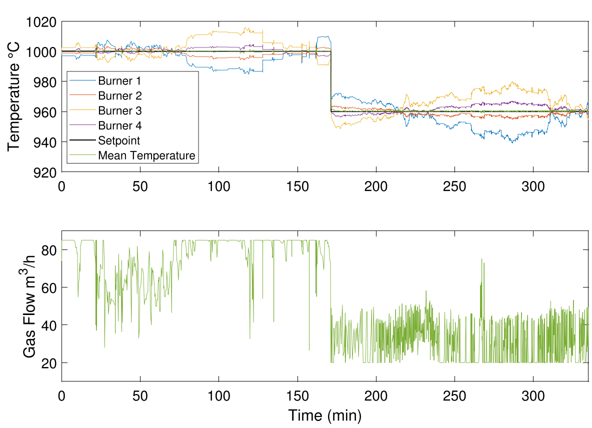

Fig. 12. Simulation results of the temperature setpoint change for the hearth 4 mean temperature control.

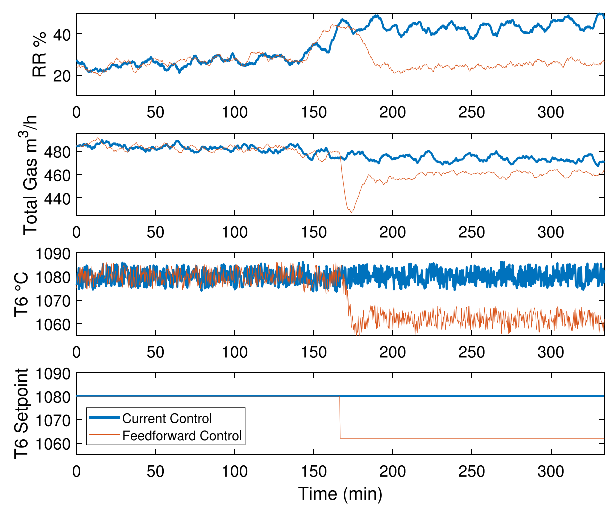

Fig. 13. Comparison of the plant current control strategy (blue) vs. the feedforward control (orange). (For interpretation of the references to color in this figure legend, the reader is referred to the web version of this article.)

achieved, as shown in Fig. 12. The mean temperature setpoint during the first half of the simulation is 1000 °C; during the second half, the mean temperature setpoint is set to 960 °C. The controlled output follows the setpoint very closely in both setpoint operations. The graph at the top of Fig. 12 illustrates the evolution of the temperatures of all burners throughout the simulation. Finally, the bottom graph shows how one gas flow of four is behaving to achieve the desired control.

5.3. Simulation of feedforward control

The feedforward controller receives the value of the reaction rate from the soft sensor as a conversion percentage from metakaolin to spinel phase calculated for the first part of the furnace (hearths 1 to 4).

Under normal process conditions, the spinel formation reaction occurs in hearth 6. Therefore, a shift in the reaction location would show as the soft-sensor values are higher than 40%. The feedforward control is activated when the conversion reaches 40% or above, and the control is kept active for 240 min in this simulation study. This control interval was implemented based on the maximum duration of the exothermic reaction, as previously reported in Section 4.2. In the practical implementation, the recommended control interval would be e.g., 40 min based on the residence time of the furnace.

Fig. 13 shows a comparison of the current control strategy, with the designed feedforward control. The variables shown in the figure are as follows: reaction rate, total gas flow, the gas temperature of hearth 6 (T6), and the gas temperature setpoint. At simulation time 150 min, the effect of the disturbance on the reaction rate can be clearly seen in the value of the conversion percentage, which increased from approximately 25% to 40%. This increase was sustained until the end of the simulation. A decrease in conversion occurred after the feedforward control was activated and the value returned to approximately 20%. As a comparison, the current control (without feedforward) did not display any changes from its setpoint of 1080 °C, being unresponsive to the

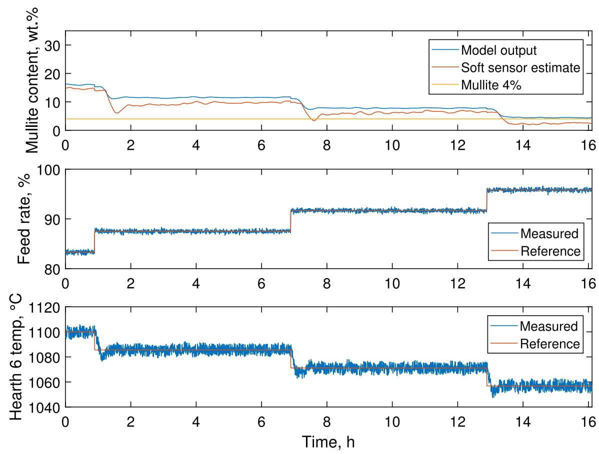

Fig. 14. Simulation of capacity optimization.

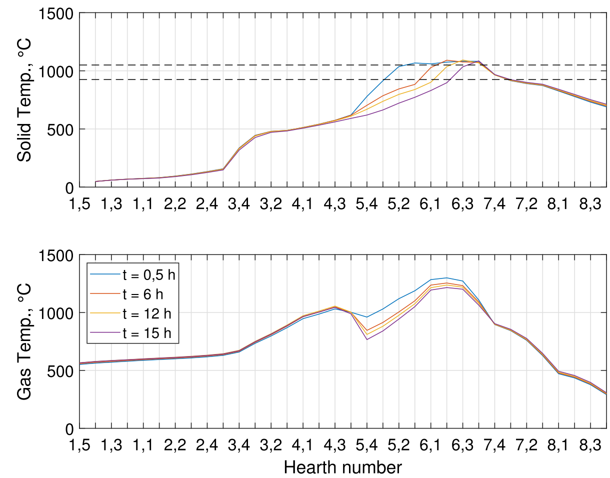

Fig. 15. Temperature profiles of gas and solid phases in the furnace at selected time instances. The hearth number is denoted by two numbers: the first is the hearth and the second is the specific volume in that hearth.

variation in reaction rate. The feedforward control presents a change at simulation time 170 min in response to the increase in conversion above 40%, thus reducing the temperature setpoint to 1062 °C. This change in setpoint was calculated using a similar approach to the reaction rate energy balance, considering the desired product quality. In the simulation study with the current control strategy of the plant, the gas consumption presented a decrease of 1.6% after the disturbances affected the process, whereas the feedforward control showed that energy savings could be nearly 3.6%.

5.4. Simulation of feed rate optimization

For evaluation, the strategy proposed in Section 4.1 was implemented in the simulation environment. First, the furnace was operated at the selected operating conditions until steady-state conditions were reached. The initial values for the feed rate optimization were as follows: the mullite content was 16%, the temperature in hearth 6 was 1100 °C, and the feed rate was 83.33%. The mullite soft-sensor output was filtered with the moving average approach, the time window being 30 min. The goal was to maintain the mullite value at approximately 4% by lowering the temperature setpoint in Hearth 6. The control interval was 6 h based on the time required for the furnace to reach the steady state, and the feed rate change was limited to 5%. Using the filtered value, the strategy determines the optimal setpoint for the feed rate and the temperature in hearth 6.

Fig. 14 shows that the control strategy increased the feed rate in this simulation study, from the initial value of 83.33% to 95.83%, and the setpoint temperature in hearth 6 was lowered by 43 °C. The graphs show a small difference between the model output and the observable soft-sensor estimate. However, the difference was considered relatively small and explained by the simplification of the soft-sensor calculations.

Fig. 15 presents in more detail the temperature profiles in the furnace for the solid and gas phases. During the control strategy testing period, the spinel formation reaction is reallocated to subsequent volumes in hearth 6. This causes a delay in the mullite formation reaction which reduces its content in the final product. In addition, the proposed optimization prevents the overheating of material above the necessary level. The dashed lines indicate the temperature interval for the spinel formation according to reaction (3). Furthermore, the results support the energy savings to the process as the gas temperature decrease in hearths 5 and 6. Additionally, the temperature of the gases changes in hearth 6 according to the specified setpoint. The same behavior is seen in hearth 5.

Thus, the capacity optimization strategy improves the throughput of the plant and reduces the energy used for calcined kaolin production.

6. Conclusion

In this study, a novel control strategy concept for the MHF was proposed. The main contribution of this manuscript is the development of two soft sensors based on the energy balance to estimate the mullite content and the "spinel-phase" reaction rate. The purpose of the calciner control system is to ensure uniform product quality while maximizing the furnace capacity and reducing the energy use. The industrially used PI-based control strategy served as a benchmark for the performance evaluation of the integrated controller. The furnace was controlled on three levels: the basic level is responsible for the basic controllers of the furnace; the stabilizing level controls the temperature profile and ensures disturbance rejection due to feed impurities; and the optimizing level focuses on maximizing capacity.

The performance and effectiveness of the proposed scheme were demonstrated through simulations using actual industrial data. Through the case studies, the control strategy can adapt to critical disturbances to the furnace (e.g., change of the feed type or impurities in the feed), such that the overall system continues to achieve its goal. In addition, the process performances are automatically optimized.

In a future study, the authors will investigate the effectiveness of this control approach across a wider variety of feed (ore) types to the calciner. Additionally, to improve the efficiency of the controller, decouplers need to be implemented. Moreover, the authors will extend the formulation to consider product quality through new instrumentation and more advanced control methods such as model predictive control.

Acknowledgments

The authors thank Imerys, S.A. for providing industrial data. The research leading to these results has received funding from the European Union Seventh Framework Programme (FP7/2013-2016) under grant agreement No. 310645. The authors also express gratitude to the Academy of Finland for the financial support received under grant agreement No. 296432.

References

Castelein, O., Soulestin, B., Bonnet, J., & Blanchart, P. (2001). The influence of heating rate on the thermal behaviour and mullite formation from a kaolin raw material. *Ceramics International*, *27*(5), 517–522. http://dx.doi.org/10.1016/S0272-8842(00)00110-3.

Eskelinen, A., Zakharov, A., Jämsä-Jounela, S.-L., & Hearle, J. (2015). Dynamic modeling of a multiple hearth furnace for kaolin calcination. *AIChE Journal*, *61*(11), 3683–3698. http://dx.doi.org/10.1002/aic.14903.

Ferron, J. R., & Singh, D. K. (1991). Rotary kiln transport processes. *AIChE Journal*, *37*(5), 747–758. http://dx.doi.org/10.1002/aic.690370512.

Fleifil, M., Lorra, M., Baukal, C. E., Lewallen, J. A., & Wright, D. E. (2006). Process burner spacing. *Petroleum Technology Quarterly*, *11*(3), 89–94.

Galvez, J., & de Araujo, L. (1996). A multivariable PI controller for nonlinear ill-conditioned electrical tubular ovens. In *Proceedings of the 39th midwest symposium on circuits and systems, Vol. 3* (pp. 1005–1008). IEEE. http://dx.doi.org/10.1109/MWSCAS.1996.592847.

Gao, Y., Glasser, B. J., Ierapetritou, M. G., Cuitino, A., Muzzio, F. J., Beeckman, J. W., et al. (2013). Measurement of residence time distribution in a rotary calciner. *AIChE Journal*, *59*(11), 4068–4076. http://dx.doi.org/10.1002/aic.14175.

Ginsberg, T., & Modigell, M. (2011). Dynamic modelling of a rotary kiln for calcination of titanium dioxide white pigment. *Computers & Chemical Engineering*, *35*(11), 2437–2446. http://dx.doi.org/10.1016/j.compchemeng.2011.03.029.

Gomez Fuentes, J. V. (2016). *Simulation environment for advanced control development of a multiple hearth furnace*. (Master's thesis), (p. 95). Aalto, URL http://urn.fi/URN:NBN:fi:aalto-201605262236.

Gouveia, R., Lewis, D., Restrepo, A., Rodrigues, L. A., & Gedraite, R. (2009). Application of model-predictive control to multi-hearth nickel reduction roasters. *IFAC Proceedings Volumes*, *42*(23), 292–296.

Jaemsae-Jounela, S.-L., Laine, S., Ruokonen, E., et al. (1998). Ore type based expert systems in mineral processing plants. *Particle & Particle Systems Characterization*, *15*(4), 200–207.

Järvensivu, M., Saari, K., & Jämsä-Jounela, S.-L. (2001). Intelligent control system of an industrial lime kiln process. *Control Engineering Practice*, *9*(6), 589–606. http://dx.doi.org/10.1016/S0967-0661(01)00017-X.

Jenkins, B., & Mullinger, P. (2013). *Industrial and process furnaces*. (p. 676). Butterworth-Heinemann.

Laine, S., Lappalainen, H., & Jämsä-Jounela, S.-L. (1995). On-line determination of ore type using cluster analysis and neural networks. *Minerals Engineering*, *8*(6), 637–648.

Langer, A. M., & Kerr, P. F. (1967). Evaluation of kaolinite and quartz differential thermal curves with a new high temperature cell. *American Mineral*, *52*, 509–523.

Liu, X., & Jiang, J. (2004). Mass and heat transfer in a continuous plate dryer. *Drying Technology*, *22*(7), 1621–1635. http://dx.doi.org/10.1081/DRT-200025619.

Martins, M. A., Oliveira, L. S., & Franca, A. S. (2001). Modeling and simulation of petroleum coke calcination in rotary kilns. *Fuel*, *80*(11), 1611–1622. http://dx.doi.org/10.1016/S0016-2361(01)00032-1.

Meisingset, H. C., & Balchen, J. G. (1995). Mathematical modeling of a rotary hearth coke calciner. *Modeling, Identification and Control: A Norwegian Research Bulletin*, *16*(4), 193–212. http://dx.doi.org/10.4173/mic.1995.4.2.

Murray, H. (2000). Clays. In *Ullmann's encyclopedia of industrial chemistry*. Weinheim, Germany: Wiley-VCH Verlag GmbH & Co. KGaA. http://dx.doi.org/10.1002/14356007.

Murray, H. H., & Kogel, J. E. (2005). Engineered clay products for the paper industry. *Applied Clay Science*, *29*(3–4), 199–206. http://dx.doi.org/10.1016/j.clay.2004.12.005.

Ptáček, P., Šoukal, F., Opravil, T., Havlica, J., & Brandštetr, J. (2011). The kinetic analysis of the thermal decomposition of kaolinite by dtg technique. *Powder Technology*, *208*(1), 20–25.

Ptáček, P., Šoukal, F., Opravil, T., Nosková, M., Havlica, J., & Brandštetr, J. (2010). The kinetics of Al–Si spinel phase crystallization from calcined kaolin. *Journal of Solid State Chemistry*, *183*(11), 2565–2569. http://dx.doi.org/10.1016/j.jssc.2010.08.030.

Ramírez, M., Haber, R., Peña, V., & Rodrŕguez, I. (2004). Fuzzy control of a multiple hearth furnace. *Computers in Industry*, *54*(1), 105–113.

Sauermann, H., Stenzel, C., Keesmann, S., & Bonduelle, B. (2001). High-stability control of multizone furnaces using optical fibre thermometers. *Crystal Research and Technology*, *36*(12), 1329. http://dx.doi.org/10.1002/1521-4079(200112)36:12<1329::AID-CRAT1329>3.0.CO;2-1.

Stadler, K. S., Poland, J., & Gallestey, E. (2011). Model predictive control of a rotary cement kiln. *Control Engineering Practice*, *19*(1), 1–9. http://dx.doi.org/10.1016/j.conengprac.2010.08.004.

Thomas, R., Grose, D., Obaje, G., Taylor, R., Rowson, N., & Blackburn, S. (2009). Residence time investigation of a multiple hearth kiln using mineral tracers. *Chemical Engineering and Processing: Process Intensification*, *48*(4), 950–954. http://dx.doi.org/10.1016/j.cep.2009.01.003.

Viljamaa, P., & Koivo, H. N. (1995). Tuning of a multivariable fuzzy logic controller. *Intelligent Automation & Soft Computing*, *1*(1), 15–28.

Voglauer, B. H., & Jörgl, P. (2004). Dynamic model of a roast process for simulation and control. *Mathematical and Computer Modelling of Dynamical Systems*, *10*(3–4), 217–230. http://dx.doi.org/10.1080/13873950412331335234.